THE JOURNAL OF
PHYSICAL CHEMISTRY
Letters

Surfaces, Interfaces, and Catalysis; Physical Properties of Nanomaterials and Materials

Unexpected Semi-Metallic BiS2 at High Pressure and High Temperature

Guangtao Liu, Zhenhai Yu, Hanyu Liu, Simon A.T. Redfern, Xiaolei Feng, Xin Li, Yuan Ye,
Ke Yang, Naohisa Hirao, Saori I. Kawaguchi, Xiaodong Li, Lin Wang, and Yanming Ma

Just Accepted

ACS Publications

1
2
3   1   **Unexpected Semi-metallic BiS₂ at High Pressure and High Temperature**
4
5   2
6
7   3
8
9   4   Guangtao Liu[1, 2, 3], Zhenhai Yu[1], Hanyu Liu[4], Simon A. T. Redfern[1, 5], Xiaolei Feng[3, 5], Xin Li[1], Ye
10
11   5   Yuan[1], Ke Yang[6], Naohisa Hirao[7], Saori Imada Kawaguchi[7], Xiaodong Li[8], Lin Wang[1, *] and
12
13   6   Yanming Ma[3,9, *]
14
15   7
16
17   8
18

9   [1] *Center for High Pressure Science and Technology Advanced Research, Shanghai 201203, China*

10   [2] *National Key Laboratory of Shock Wave and Detonation Physics, Institute of Fluid Physics, China*

11   *Academy of Engineering Physics, Mianyang 621900, China*

12   [3] *State Key Laboratory of Superhard Materials, College of Physics, Jilin University, Changchun*

13   *130012, China*

14   [4] *Geophysical Laboratory, Carnegie Institution of Washington, Washington, DC 20015, USA*

15   [5] *Department of Earth Sciences, University of Cambridge, Downing Street, Cambridge, CB2 3EQ,*

16   *UK*

17   [6] *Shanghai Institute of Applied Physics, Chinese Academy of Sciences, Shanghai 201203, China*

18   [7] *Japan Synchrotron Radiation Research Institute, 1-1-1 Kouto, Sayo-cho, Sayo-gun, Hyogo*

19   *679-5198, Japan*

20   [8] *Institute of High Energy Physics, Chinese Academy of Sciences, Beijing 100049, China*

21   [9] *International Center of Future Science, Jilin University, Changchun 130012, China*

22

23

24   **Corresponding authors:** wanglin@hpstar.ac.cn (Prof. Lin Wang) and mym@jlu.edu.cn (Prof.

25   Yanming Ma)

26

Abstract

In the last decade, the group V-VI compounds have been widely investigated due to their excellent properties and applications. It is now accepted that diverse stoichiometry can yield new compounds with unanticipated properties, uncovering potentially new physicochemical mechanisms. However, in this group, aside from the conventional A_2B_3-type, no other energetically stable stoichiometry has been reported yet. Here, we report that Bi_2S_3 is unstable and decomposes into stoichiometric BiS_2 and BiS with different Bi valence states upon compression. Encouragingly, we successfully synthesized the predicted BiS_2 phase and thus, confirmed its existence. Our current calculations reveal that the found BiS_2 phase is a semi-metal, associated with the increased concentration of nonmetallic S. The present results represent the first counterintuitive stable stoichiometry of group V-VI and provide a good example in designing and synthesizing new compounds under compression.

Table of Contents
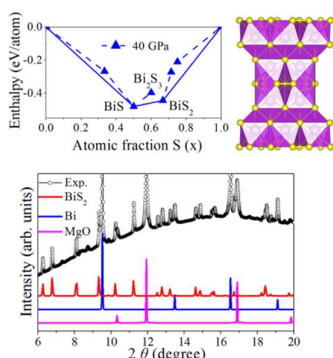
The calculated phase diagram and synthesized BiS_2 compound.

45   The group V-VI compounds, which are important both in practical applications and in

46   fundamental science, have attracted significant research interest in recent years. The Bi_2Te_3 and

47   Sb_2Te_3 alloys are by far the most widely used thermoelectric materials[1]. Bi_2S_3 is a typical

48   semiconductor with a direct bandgap of ~1.3-1.9 eV[2,3] and is widely used in thermoelectric[4],

49   electronic[5], and optoelectronic devices[6]. Bi_2Se_3, Bi_2Te_3, and Sb_2Te_3 were especially predicted to be

50   the simplest 3-dimensional topological insulators[7] and this was subsequently experimentally

51   confirmed[8]. It is well-known that compression can significantly alter the properties of matter, driving

52   increased density via largely changing atomic distance, bonding, and stacking symmetry. It may also

53   induce charge transfer or alter the spin state of a material, and thus, drive phase transitions.

54   High-pressure studies have been carried out to extensively tailor the properties of the group V-VI

55   compounds. For instance, the thermoelectric properties of Bi_2Te_3 and Sb_2Te_3 can be significantly

56   enhanced by high pressure[9,10]. The superconductivity was observed between 3 and 6 GPa in Bi_2Te_3[11]

57   and shows pressure-dependence, which has been correlated to its high-pressure phase transitions[12].

58   Subsequently, it was reported that Bi_2Te_3 undergoes a series of structural phase transitions and finally

59   forms a disordered cubic alloy[13,14]. The similar high-pressure phase transitions have also been

60   observed in Sb_2Te_3[15,16] and Bi_2Se_3[17–19]. At ambient pressure, Bi_2S_3 crystallizes in an orthorhombic

61   structure (*Pnma*)[20], in which Bi is irregularly coordinated by S in two distinct crystallographic sites,

62   with irregular 7- and 8-fold coordination. High-pressure X-ray diffraction (XRD) studies found that

63   Bi_2S_3 has a possible second-order isosymmetric transition around 4-6 GPa and retains *Pnma*

64   symmetry up to 50 GPa[21]. Furthermore, a pressure-induced semiconductor-metal transition in Bi_2S_3

65   has been indicated under compression[22].

66   The search for the new stoichiometry of a compound plays an important role in determining

67   materials and even improving their properties. Many recent studies have proven that pressure is a

68   very effective tool to synthesize new stoichiometric compounds that are generally inaccessible at

69   ambient conditions[23–25]. Thus, irreplaceable pressure enables us to explore more physical and

70   chemical processes that illuminate our understanding of the nature of solids more generally. However,

71   besides the well-known A_2B_3-type and some metastable phases, no other energetically stable

72   stoichiometry has been reported in such a significant system thus far. Therefore, it is anticipated that

73   the group V-VI compounds with different stoichiometries have further novel phenomena.

74   Here, we investigate the possibility that other, as yet unknown, stable compounds exist in the

75 group V-VI compounds. Initially, the Bi-S system was chosen to study as a general representative.

76 Variable chemical compositions of Bi_xS_y have been explored using the crystal structure prediction

77 method under high pressures. The enthalpy calculations indicate that Bi_2S_3 is thermodynamically

78 unstable and tends to spontaneously decompose above 24 GPa into two new stoichiometric phases

79 BiS_2 and BiS, which have abnormal valence states and are stable above 9 and 19 GPa, respectively.

80 Using the diamond anvil cell (DAC) and laser heating techniques, our subsequent experiment

81 confirmed the predicted BiS_2 phase, revealing an interesting semi-metallic behavior.

82

83 The formation enthalpy of each stoichiometric Bi_xS_y is defined as

84 $H_{f/atom} = \frac{H_{Bi_xS_y/f.u.} - x\,H_{Bi/atom} - y\,H_{S/atom}}{x+y}$, where the *R-3m* and *Im-3m* phases[26] were used for Bi, and

85 the *Fddd*, *P3$_2$21* and *I4$_1$/acd* phases[27] were employed for S as the endpoint compositions at

86 corresponding pressures. To validate our computational scheme for the Bi-S system, we successfully

87 reproduced the known orthorhombic phase of Bi_2S_3 at both atmospheric pressure and 10 GPa using

88 the crystal structure prediction method[28,29], as well as its equation of state (EOS), verifying the

89 reliability of the methodology. We then extended our structure searches to consider other

90 stoichiometries. The enthalpic convex hulls, showing enthalpies as function of pressure, are

91 summarized in Figure 1, where the points on the convex extrema are energetically stable

92 stoichiometries. At ambient pressure, we found that only Bi_2S_3 exists (Fig. 1a), in agreement with the

93 actual observation and thus, confirming the reliability of our computational scheme. It can be seen

94 that the stability of Bi_xS_y changes at elevated pressures (Figs. 1b and 1c). As anticipated, not only

95 Bi_2S_3, but also new stoichiometric BiS_2 and BiS become energetically stable above 9 and 19 GPa,

96 respectively (Fig. 1d). More unexpectedly, it is apparent that conventional Bi_2S_3 is energetically
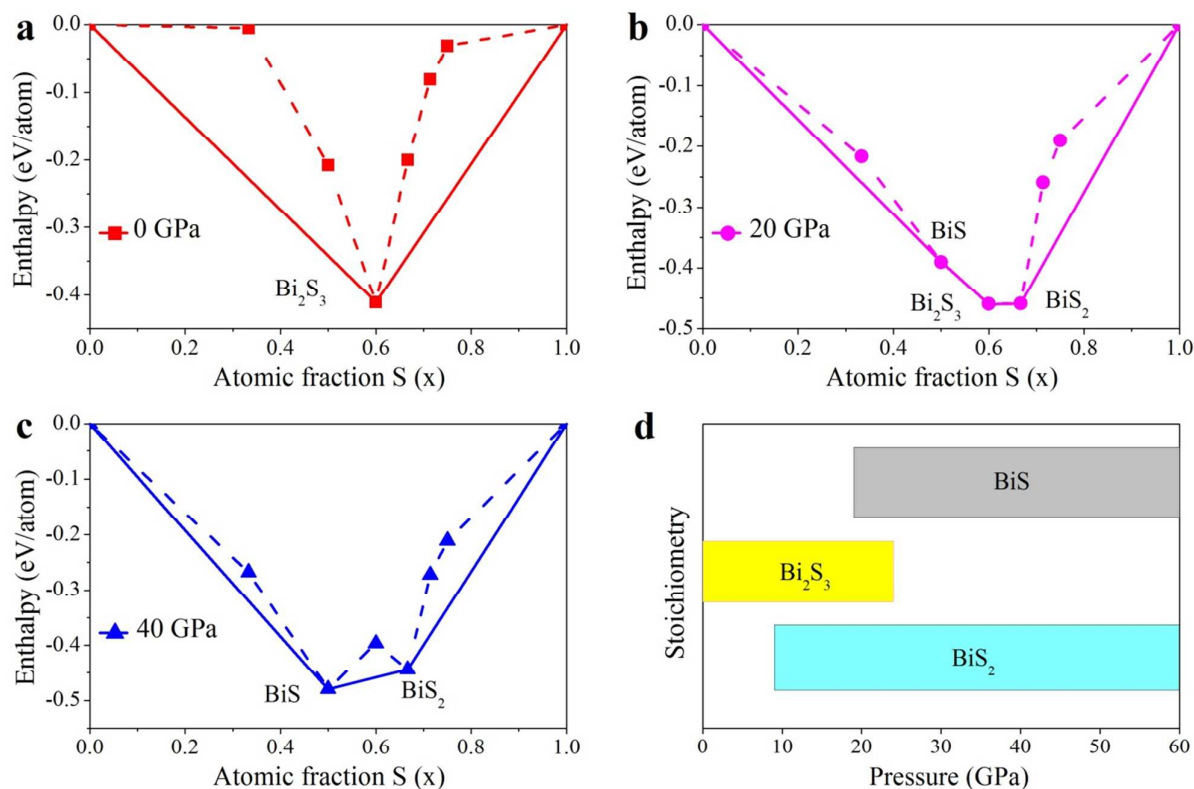
97 unstable above 24 GPa and tends to decompose.

98

99   Fig. 1: Ground-state and static enthalpy of the formation per atom of $Bi_{1-x}S_x$ structures with respect

100 to their end-member compositions; the sulfur molar content ($x = 0$ corresponds to pure Bi; $x = 1$ to

101 pure S) for the ground state and P = (**a**) 0, (**b**) 20, and (**c**) 40 GPa. The symbols on the solid lines

102 denote that the compounds that we have identified to be stable at the corresponding pressures, while

103 those on the dashed lines represent those that are unstable with respect to decomposition into

104 elements and other stable compounds. (**d**) The stable stoichiometries and their stable range of

105 pressure.

106

107   To confirm the dynamical stabilities of the predicted phases, we also calculated the phonon

108 dispersions of BiS and BiS_2. No imaginary phonon frequency was found across the Brillouin zone

109 (BZ), confirming the dynamic stability of BiS (Fig. S1a). In addition, the phonon calculations reveal

110 that the found $P2/m$ structure (BiS_2) through the modulation of a soft phonon mode (Fig. S1b) is

111 dynamically stable (Fig. S1c). On the other hand, *ab initio* molecular dynamics simulations also

112 show that this structure experiences no additional structural change upon relaxation, since there is no

113 energy shift in a total 10 ps simulation. (Fig. S2) Therefore, we conclude that the modulated $P2/m$

114   structure is the ground-state structure of BiS_2 phase under high pressure.

115   The stable crystal structures of each stoichiometry within the Bi-S binary at 20 GPa are shown in

116   Figure 2. The familiar Bi_2S_3 phase is composed of stacked irregular $BiS_{7/8}$ co-ordination polyhedra

117   (Fig. 2a). The simple cubic (sc) BiS (*Pm-3m*) phase, on the other hand, comprises stacked regular

118   BiS_8 hexahedra (Fig. 2b). Finally, a monoclinic BiS_2 phase is formed by BiS_9 triskaidecahedra, and

119   can   be   described   as   a   layer-liked   structure   with   a   stacking

120   sequence $\cdots$S-Bi-S-S-Bi-S-Bi-S-S-Bi-S$\cdots$ along the *b*-axis (Fig. 2c).

121

Bi₂S₃ (*Pnma*)   BiS (*Pm-3m*)   BiS₂ (*P2/m*)
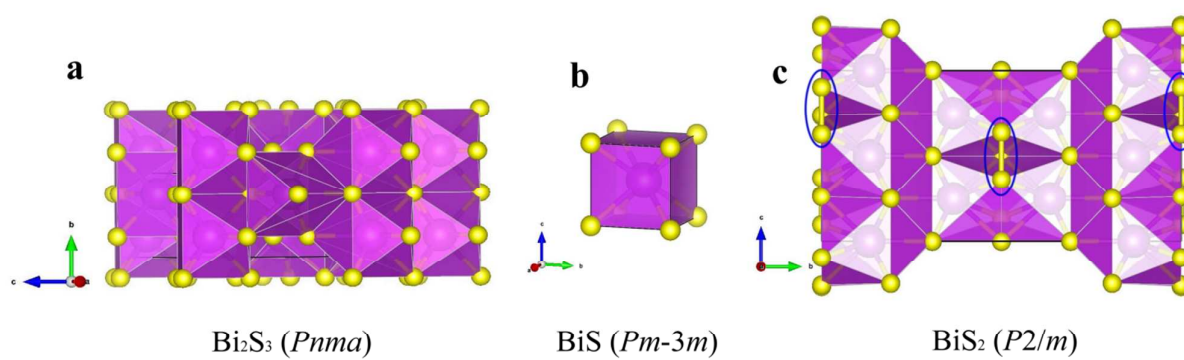
122

123   Fig. 2: The schematic crystal structures of (**a**) Bi_2S_3 (*Pnma*), (**b**) BiS (*Pm-3m*), and (**c**) BiS_2 (*Cmca*)

124   at 20 GPa. Large purple and small yellow spheres represent the Bi and S atoms, respectively. The

125   S-S bond is indicated within the blue ellipses.

126

127   In order to confirm the theoretically predicted stoichiometries given by our *ab initio*

128   computational results, further high-pressure experiments were performed to synthesize samples

129   across the Bi-S composition range. The structure search results indicate that Bi_2S_3 should decompose,

130   and layered BiS_2 can be synthesized more easily under compression since it has relatively low

131   enthalpy in the convex hull (Fig. 1). Thus, we tried to obtain BiS_2 at extreme conditions along these

132   two designed pathways: (i) $Bi_2S_3 \rightarrow \frac{1}{2}Bi + \frac{3}{2}BiS_2$ and (ii) $Bi + 2\,S \rightarrow BiS_2$. In the first run, the

133   starting material was a well-characterized sample of Bi_2S_3, which was checked carefully before

134   heating to confirm the absence of any Bi impurity (Fig. S3). The sample was compressed to 38 GPa

135   and heated up to about 2000 K for 30 minutes. The pressure was then decreased to 31.5 GPa after

136 laser heating. The quenched sample was scanned by an X-ray beam to investigate any heterogeneity

137 caused by the temperature gradient of laser heating. XRD mapping results showed that many new

138 grains had formed with a typical length scale of several μm. We note that the experimental intensities

139 of the XRD patterns were dominated by obvious texture and pseudo-single crystal statistics after the

140 experiments, which had provoked rather coarse recrystallization from high temperature. However,

141 clear diffraction peaks of a body centered cubic (bcc) structure were observed in certain parts of the

142 sample, which were identified as the high-pressure phase of Bi. In addition to Bi, at least two

143 additional phases existed. Using the results of our computations we were able to test these structures

144 against our predictions, and conclude that the original Bi_2S_3 sample may have decomposed into a

145 mixture of Bi and BiS_2. Apart from a few unidentified peaks, most of the diffraction patterns at 31.5

146 GPa can be attributed to a mixture of BiS_2 and Bi, (Fig. 3a). The residual unidentified peaks may be

147 from an additional metastable phase(s) that have yet to be identified or are possibly explained by

148 other stoichiometry beyond our current calculations. For the second run, we heated a mixture of

149 elemental Bi and S at 39 GPa to synthesize BiS_2. We successfully synthesized the BiS_2 phase again

150 and obtained correspondingly high quality diffraction data (Fig. S4). The representative plots with

151 the calculated versus experimental diffraction profiles (Fig. 3b), as well as the refinement (Fig. 3c),

152 clearly demonstrate the presence of BiS_2.

153
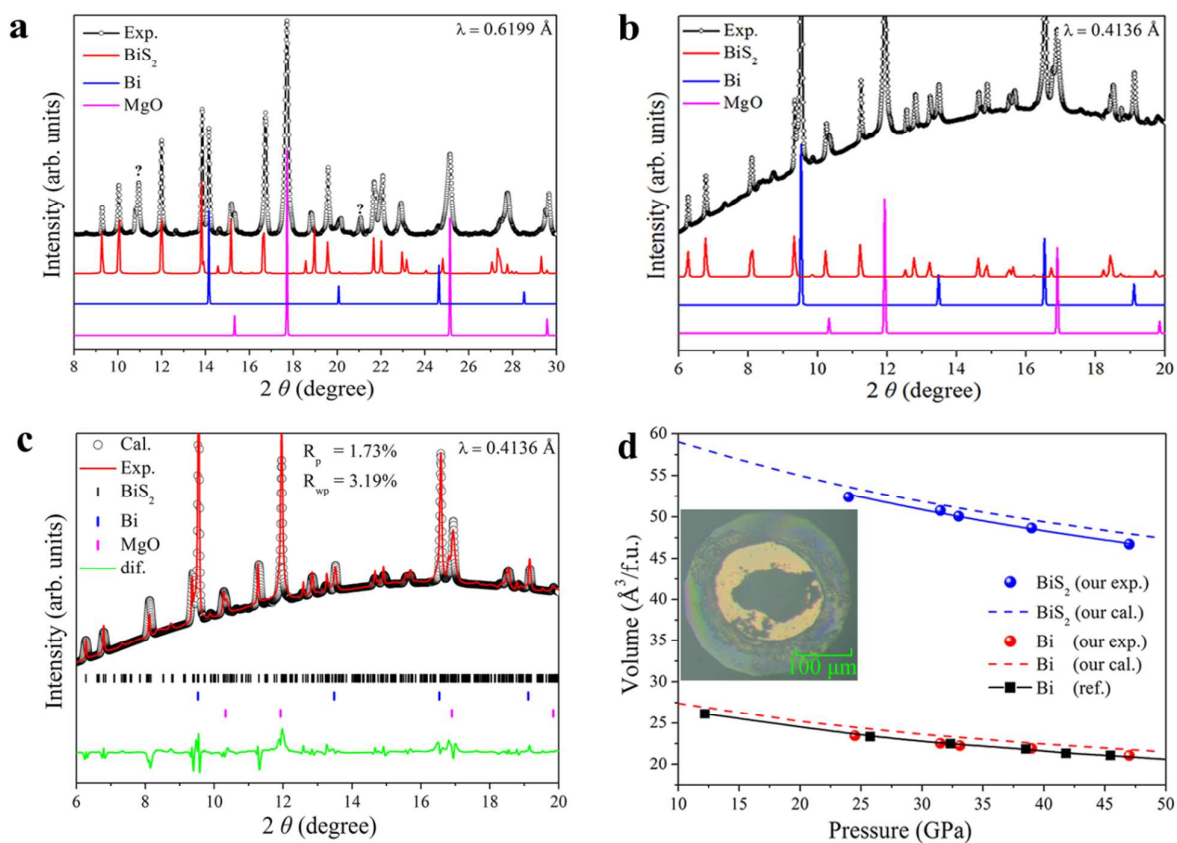
Fig. 3: The experimental XRD pattern and the calculated diffraction peaks of BiS_2, Bi and MgO at (**a**)
154

31.5 and (**b**) 39 GPa. The unidentified diffraction peaks with question marks are from undefined
155

phases. (**c**) The diffraction refinement at 39 GPa. The black open circles and red solid line represent
156

the Rietveld fits and observed data, respectively. (**d**) The red and blue points represent our
157

experimental volumes of Bi and BiS_2 as function of pressure compared with our calculated EOSs.
158

The black solid line is the previous EOS of Bi from the reference[31]. The inset shows the compressed
159

sample in the DAC.
160

161

The calculated and fitted experimental third order Birch–Murnaghan EOSs[30] of Bi and BiS_2 are
162

plotted in Figure 3d. Our experimental data of Bi are well consistent with the previous reference[31].
163

Since general gradient approximation normally overestimates the lattice parameters, it is reasonable
164

that our calculated volumes are slightly larger than the experimental values. We found that the
165

reported BiS_2 phase is denser and more incompressible than the familiar phase of Bi_2S_3, as indicated
166

by comparing their EOSs and bulk moduli (Fig. S5). Typically, compression results in crystalline
167

168 materials becoming denser and tending towards close-packed arrangements at high pressure, with a

169 concomitant increase in the coordination number of the atoms or ions. Our results show that, in these

170 Bi-S compounds, the coordination of Bi by S increases from 7 or 8 (Bi_2S_3) to 9 (BiS_2). However, this

171 increase in coordination number results in an increase in the average bond length, despite the

172 increase in pressure. For example, at 20 GPa the inter-atomic distance of the Bi-S bond changes from

173 2.68-2.75 Å in Bi_2S_3 to 2.75-2.96 Å in BiS_2. This can be understood in terms of the increased

174 repulsive interactions between nearest neighbor atoms arising from the increase in the number of

175 coordinating S atoms. Interestingly, we observed that covalent S-S bonds exist in BiS_2, as seen in

176 Figure 2c, with a bond length of 2.04 Å which is exceedingly close to the value (2.08 Å) for the S-S

177 covalent bond seen in the chain-structure of elemental S-II ($P3_221$) at 20 GPa. Our additional

178 electron localized function calculation confirms that the adjacent S atoms show a typical covalent

179 bond character (Fig. S6), which has not been observed in other metal sulfides before.

180 Since it is difficult to obtain pure phases from DAC synthesis, electronic properties were

181 investigated using first principles calculations. Because DFT usually underestimates the bandgap of

182 materials, we employed the screened hybrid functional of Heyd, Scuseria, and Ernzerhof (HSE06)[32]

183 to better describe its band structure and density of states (DOS). In BiS (Fig. 4a), the valence bands

184 and conduction bands completely overlap indicating a metallic state with superconductivity (Fig. S7).

185 The valence band of BiS_2 is occupied by S_$3p$ (Fig. 4b). It can be seen that there is slight overlap

186 along the Γ-Y direction and that the DOS is near zero at the Fermi level, indicating that BiS_2 is an

187 interesting semi-metallic phase. And this semi-metallic state remains under higher pressure (40 GPa),

188 which is different from the normal metallic behavior of group V-VI compounds under compression.

189 The diverse electronic properties can be understood intuitively in terms of the different

190 concentrations of nonmetallic S in these phases, which can lead to an increase in valence electron

191 transfer from Bi to S in BiS_2.
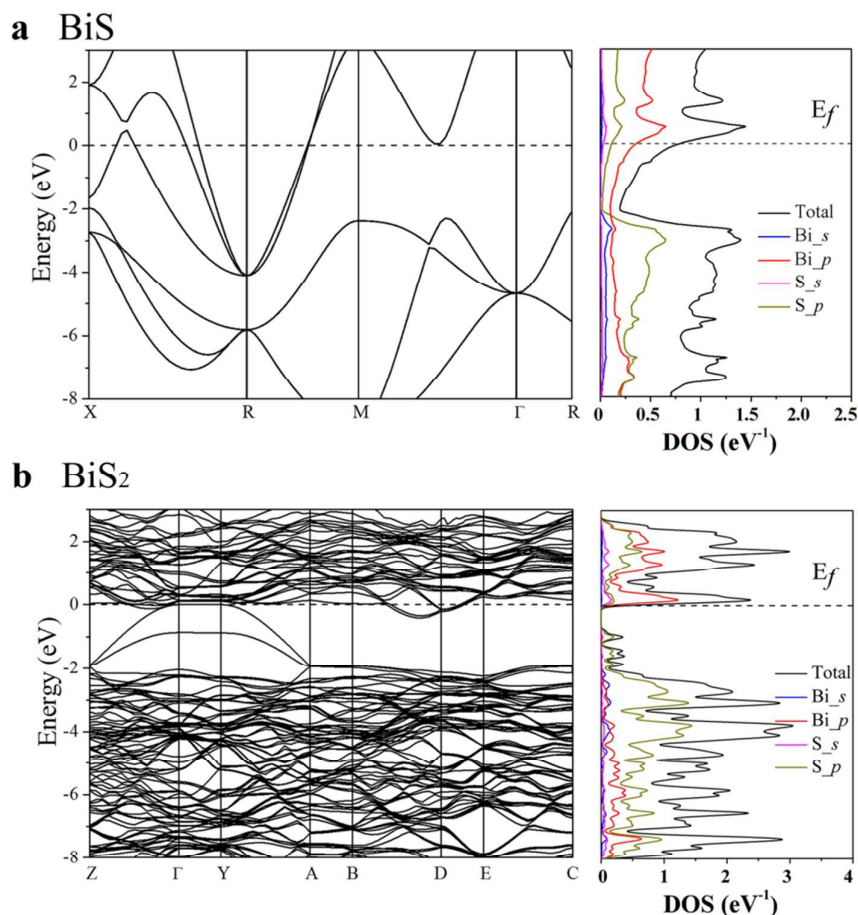
a BiS

b BiS₂

Fig. 4: Band structures along high symmetry paths and the projected DOSs of (**a**) BiS and (**b**) BiS$_2$ at 20 GPa. The Fermi level has been set to 0 eV.

High-pressure and high-temperature techniques are particularly valuable in the search for such structural variability. We note that the ambient Bi$_2$S$_3$ phase was robust at room temperature and high pressure[21], and only BiS$_2$ was synthesized in our experiments. Its synthesis pressure was higher than that suggested by the structure prediction calculations. The hysteresis of chemical reaction may be a result of the activation energies associated with experimental synthesis methods and the unclear pathway (during synthesis) across the potential energy surface in this system, which often occurs in many other experimental cases. The new structure should not only be thermodynamically and dynamically stable, but also the energy barrier needs to be overcome in the actual experiment. Thus, plenty of anticipated materials can be obtained only at extreme conditions. Since BiS becomes energetically favored at higher pressure, we reasonably conjecture that stoichiometric BiS can also

10

206 be synthesized, once the barrier is overcome at higher pressure (compared with the theoretical one)

207 or temperature. Our work on the Bi-S system encourages us to believe that, as well as the

208 well-known A_2B_3-structure type, other undiscovered phases with interesting and potentially useful

209 properties should exist among the group V-VI compounds, which can be engineered or controlled by

210 tuning these compositions under compression and have been confirmed by our primary calculations

211 (Fig. S8). It should be noted that variations of stoichiometry need to be carefully considered in

212 high-pressure calculations and experimental studies, which can significantly enrich materials with

213 undetected properties and potential applications.

214   In summary, we carried out systematic simulations on compounds that exist across the Bi-S

215 binary system using a crystal structure prediction approach under high pressure. Two new

216 stoichiometric BiS_2 and BiS compounds were predicted to be stable above ~9 and 19 GPa,

217 respectively, whereas conventional Bi_2S_3 was found to decompose above 24 GPa, as we have

218 verified through synchrotron XRD experiments in a laser-heated DAC. 8-fold coordinated sc BiS and

219 layered 9-fold coordinated BiS_2 are more densely packed compared with 7/8-fold coordinated Bi_2S_3.

220 Other than +3, Bi shows a rich variety of valence states under compression. Electronic structure

221 calculations indicate that the newly-uncovered BiS_2 phase shows interesting semi-metallic behavior.

222 The present results demonstrate that, as well as the familiar A_2B_3-type compound, other unexpected

223 stoichiometries are stable in group V-VI at high pressure. High-pressure studies can provide new

224 insights into the design, exploration, and ultimately synthesis of novel materials with unusual

225 chemistry and potentially useful properties.

226

227

Methods

228   The crystal structures of Bi-S compounds were systematically probed using the Crystal structure

230   AnaLYsis by Particle Swarm Optimization (CALYPSO) code[28,29]. This method has been applied

231   successfully to a wide range of crystalline systems ranging from elemental solids to binary and

232   ternary pounds[33–36]. The simulation cell comprised 1-8 f.u. (equivalent to 24 atoms) with 6

233   stoichiometries (Bi_2S, BiS, Bi_2S_3, BiS_2, Bi_2S_5, and BiS_3) at 0, 10, 30, and 60 GPa. DFT calculations,

234   including structural optimizations, enthalpies, electronic structures and phonons, were performed

235   with Vienna Ab initio Simulation Package (VASP)[37] code using the Perdew-Burke-Ernzerhof[38]

236   exchange-correlation functional. The $6s^2 6p^3$ and $3s^2 3p^4$ electrons were treated as valence electrons

237   for Bi and S, respectively. To ensure that all enthalpy calculations were well converged to about 1

238   meV/atom, a Monkhorst-Pack grid was selected with sufficient density ($2\pi \times 0.02$ Å^{-1}) in reciprocal

239   space, as well as an appropriate energy cutoff (350 eV). The phonon calculations and modulations of

240   the soft phonon modes were carried out using a finite displacement approach[39] through the

241   PHONOPY code[40].

242   High-pressure/high-temperature synthesis experiments were carried out using a laser-heated

243   symmetric DAC with culets diameter of 300 μm. Bi_2S_3 powder (Alfa Aesar, 99.9%) in the first run

244   and mixed Bi/S (Alfa Aesar, 99.99%/99.5%) in the second run were prepressed into thin sheets (~10

245   μm) and then loaded between two layers of MgO to form a sandwich structure, where MgO was used

246   as both the thermal insulator and pressure medium. Pressures were determined by the ruby

247   fluorescence method[41]. An ytterbium fiber laser (1064 nm excitation line) with a beam size of ~50

248   μm was used to heat the sample from both sides. The laser installed in BL10XU is SPI fiber laser

249   with 1050 nm. Temperatures were measured by fitting the visible portion of the black-body radiation

250   from the heating spot on the sample to the Planck radiation function.

251   *In situ* high-pressure angle-dispersive XRD experiments at room temperature were performed

252   principally at beamline 15U1 (0.6199 Å) of the Shanghai Synchrotron Radiation Facility and

253   beamline 10XU (0.4136 Å) of SPring8. Some additional experiments were conducted at the 4W2

254   High Pressure Station of the Beijing Synchrotron Radiation Facility. The sample to detector distance

255   and other geometric parameters were calibrated using a CeO_2 standard. The software package

256   Dioptas[42] was used to integrate powder diffraction rings and convert the 2-dimensional data to

257   1-dimensional profiles. The resulting diffraction patterns were refined via Rietveld refinement using

258 the GSAS package[43].

259

266

Supporting Information

268   The Supporting Information is available XXX.

269 Phonon dispersion curves, MD simulation, Diffraction patterns, EOS, ELF, Electron phonon

270 coupling calculation and details of the crystal structures.

271

272 **References**

273

274 (1) Snyder, G. J.; Toberer, E. S. Complex Thermoelectric Materials. *Nat. Mater.* **2008**, *7*, 105–

275   114.

276 (2) Sharma, Y.; Srivastava, P.; Dashora, A.; Vadkhiya, L.; Bhayani, M. K.; Jain, R.; Jani, A. R.;

277   Ahuja, B. L. Electronic Structure, Optical Properties and Compton Profiles of Bi_2S_3 and

278   Bi_2Se_3. *Solid State Sci.* **2012**, *14* (2), 241–249.

279 (3) Filip, M. R.; Patrick, C. E.; Giustino, F. GW Quasiparticle Band Structures of Stibnite,

280   Antimonselite, Bismuthinite, and Guanajuatite. *Phys. Rev. B* **2013**, *87* (20), 205125.

281 (4) Du, X.; Cai, F.; Wang, X. Enhanced Thermoelectric Performance of Chloride Doped Bismuth

282   Sulfide Prepared by Mechanical Alloying and Spark Plasma Sintering. *J. Alloys Compd.* **2014**,

283   *587*, 6–9.

284 (5) Huang, X.; Yang, Y.; Dou, X.; Zhu, Y.; Li, G. In Situ Synthesis of Bi/Bi2S3 Heteronanowires

285   with Nonlinear Electrical Transport. *J. Alloys Compd.* **2008**, *461* (1–2), 427–431.

286 (6) Wang, Y.; Chen, J.; Jiang, L.; Sun, K.; Liu, F.; Lai, Y. Photoelectrochemical Properties of

287   Bi2S3 Thin Films Deposited by Successive Ionic Layer Adsorption and Reaction (SILAR)

288   Method. *J. Alloys Compd.* **2016**, *686*, 684–692.

289 (7) Zhang, H.; Liu, C.-X.; Qi, X.-L.; Dai, X.; Fang, Z.; Zhang, S.-C. Topological Insulators in

290   Bi_2Se_3, Bi_2Te_3 and Sb2Te3 with a Single Dirac Cone on the Surface. *Nat. Phys.* **2009**, *5* (6),

291   438–442.

292 (8) Chen, Y. L.; Analytis, J. G.; Chu, J.-H.; Liu, Z. K.; Mo, S.-K.; Qi, X. L.; Zhang, H. J.; Lu, D.

293   H.; Dai, X.; Fang, Z.; et al. Experimental Realization of a Three-Dimensional Topological

294   Insulator, Bi_2Te_3. *Science.* **2009**, *325* (5937), 178–181.

295 (9) Ovsyannikov, S. V.; Shchennikov, V. V. High-Pressure Routes in the Thermoelectricity or

296   How One Can Improve a Performance of Thermoelectrics. *Chem. Mater.* **2010**, *22* (3), 635–

297   647.

298 (10) Ovsyannikov, S. V.; Shchennikov, V. V.; Vorontsov, G. V.; Manakov, A. Y.; Likhacheva, A.

299   Y.; Kulbachinskii, V. A. Giant Improvement of Thermoelectric Power Factor of Bi_2Te_3 under

300   Pressure. *J. Appl. Phys.* **2008**, *104* (5), 053713.

301 (11) Zhang, J. L.; Zhang, S. J.; Weng, H. M.; Zhang, W.; Yang, L. X.; Liu, Q. Q.; Feng, S. M.;

302   Wang, X. C.; Yu, R. C.; Cao, L. Z.; et al. Pressure-Induced Superconductivity in Topological

303   Parent Compound Bi_2Te_3. *Proc. Natl. Acad. Sci. U. S. A.* **2011**, *108*, 24–28.

304   (12) Zhang, C.; Sun, L.; Chen, Z.; Zhou, X.; Wu, Q.; Yi, W.; Guo, J.; Dong, X.; Zhao, Z. Phase

305   Diagram of a Pressure-Induced Superconducting State and Its Relation to the Hall Coefficient

306   of Bi_2Te_3 Single Crystals. *Phys. Rev. B* **2011**, *83* (14), 140504.

307   (13) Zhu, L.; Wang, H.; Wang, Y.; Lv, J.; Ma, Y.; Cui, Q.; Ma, Y.; Zou, G. Substitutional Alloy of

308   Bi and Te at High Pressure. *Phys. Rev. Lett.* **2011**, *106*, 145501.

309   (14) Einaga, M.; Ohmura, A.; Nakayama, A.; Ishikawa, F.; Yamada, Y.; Nakano, S.

310   Pressure-Induced Phase Transition of Bi_2Te_3 into the Bcc Structure. *Phys. Rev. B* **2011**, *83* (9),

311   092102.

312   (15) Zhao, J.; Liu, H.; Ehm, L.; Chen, Z.; Sinogeikin, S.; Zhao, Y.; Gu, G. Pressure-Induced

313   Disordered Substitution Alloy in Sb_2Te_3. *Inorg. Chem.* **2011**, *50*, 11291–11293.

314   (16) Ma, Y.; Liu, G.; Zhu, P.; Wang, H.; Wang, X.; Cui, Q.; Liu, J.; Ma, Y. Determinations of the

315   High-Pressure Crystal Structures of Sb_2Te_3. *J. Phys. Condens. Matter* **2012**, *24*, 475403.

316   (17) Vilaplana, R.; Santamaría-Pérez, D.; Gomis, O.; Manjón, F. J.; González, J.; Segura, A.;

317   Muñoz, A.; Rodríguez-Hernández, P.; Pérez-González, E.; Marín-Borrás, V.; et al. Structural

318   and Vibrational Study of Bi_2Se_3 under High Pressure. *Phys. Rev. B* **2011**, *84* (18), 184110.

319   (18) Liu, G.; Zhu, L.; Ma, Y.; Lin, C.; Liu, J.; Ma, Y. Stabilization of 9/10-Fold Structure in

320   Bismuth Selenide at High Pressures. *J. Phys. Chem. C* **2013**, *117* (19), 10045–10050.

321   (19) Yu, Z.; Wang, L.; Hu, Q.; Zhao, J.; Yan, S.; Yang, K.; Sinogeikin, S.; Gu, G.; Mao, H.

322   Structural Phase Transitions in Bi_2Se_3 under High Pressure. *Sci. Rep.* **2015**, *5* (1), 15939.

323   (20) Kyono, A.; Kimata, M. Structural Variations Induced by Difference of the Inert Pair Effect in

324   the Stibnite-Bismuthinite Solid Solution Series $(Sb,Bi)_2S_3$. *Am. Mineral.* **2004**, *89* (7), 932–

325   940.

326   (21) Efthimiopoulos, I.; Kemichick, J.; Zhou, X.; Khare, S. V; Ikuta, D.; Wang, Y. High-Pressure

327   Studies of Bi_2S_3. *J. Phys. Chem. A* **2014**, *118*, 1713.

328   (22) Li, C.; Zhao, J.; Hu, Q.; Liu, Z.; Yu, Z.; Yan, H. Crystal Structure and Transporting Properties

329   of Bi_2S_3 under High Pressure: Experimental and Theoretical Studies. *J. Alloys Compd.* **2016**,

330   *688*, 329–335.

331   (23) Zhang, W.; Oganov, A. R.; Goncharov, A. F.; Zhu, Q.; Boulfelfel, S. E.; Lyakhov, A. O.;

Stavrou, E.; Somayazulu, M.; Prakapenka, V. B.; Konopkova, Z. Unexpected Stable Stoichiometries of Sodium Chlorides. *Science.* **2013**, *342*, 1502–1505.

(24) Drozdov, A. P.; Eremets, M. I.; Troyan, I. A.; Ksenofontov, V.; Shylin, S. I. Conventional Superconductivity at 203 Kelvin at High Pressures in the Sulfur Hydride System. *Nature* **2015**, *525*, 73–76.

(25) Hu, Q.; Kim, D. Y.; Yang, W.; Yang, L.; Meng, Y.; Zhang, L.; Mao, H. K. FeO_2 and FeOOH under Deep Lower-Mantle Conditions and Earth's Oxygen-Hydrogen Cycles. *Nature* **2016**, *534* (7606), 241–244.

(26) Aoki, K.; Fujiwara, S.; Kusakabe, M. Stability of the Bcc Structure of Bismuth at High Pressure. *Journal of the Physical Society of Japan*. 1982, pp 3826–3830.

(27) Degtyareva, O.; Gregoryanz, E.; Mao, H.-K.; Hemley, R. J. Crystal Structure of Sulfur and Selenium at Pressures up to 160 GPa. *High Press. Res.* **2005**, *25* (1), 17–33.

(28) Wang, Y.; Lv, J.; Zhu, L.; Ma, Y. Crystal Structure Prediction via Particle-Swarm Optimization. *Phys. Rev. B* **2010**, *82* (9), 094116.

(29) Wang, Y.; Lv, J.; Zhu, L.; Ma, Y. CALYPSO: A Method for Crystal Structure Prediction. *Comput. Phys. Commun.* **2012**, *183* (10), 2063–2070.

(30) Birch, F. Finite Elastic Strain of Cubic Crystals. *Phys. Rev.* **1947**, *71*, 809–824.

(31) *Y. Akahama, M. Kobayashi, and H. Kawamura, Proceeding of 31st High Pressure Conference of Japan, Osaka, Japan, 1990, Pp. 392–393.*

(32) Heyd, J.; Scuseria, G. E.; Ernzerhof, M. Hybrid Functionals Based on a Screened Coulomb Potential. *J. Chem. Phys.* **2003**, *118* (18), 8207–8215.

(33) Lv, J.; Wang, Y.; Zhu, L.; Ma, Y. Predicted Novel High-Pressure Phases of Lithium. *Phys. Rev. Lett.* **2011**, *106*, 015503.

(34) Liu, G.; Besedin, S.; Irodova, A.; Liu, H.; Gao, G.; Eremets, M.; Wang, X.; Ma, Y. Nb-H System at High Pressures and Temperatures. *Phys. Rev. B* **2017**, *95* (10), 104110.

(35) Zhang, M.; Liu, H.; Li, Q.; Gao, B.; Wang, Y.; Li, H.; Chen, C.; Ma, Y. Superhard BC_3 in Cubic Diamond Structure. *Phys. Rev. Lett.* **2015**, *114*, 015502.

(36) Li, Y.; Hao, J.; Liu, H.; Lu, S.; Tse, J. S. High-Energy Density and Superhard Nitrogen-Rich B-N Compounds. *Phys. Rev. Lett.* **2015**, *115*, 105502.

(37) Kresse, G.; Furthmüller, J. Efficient Iterative Schemes for Ab Initio Total-Energy Calculations

362　　　　Using a Plane-Wave Basis Set. *Phys. Rev. B* **1996**, *54*, 11169–11186.

363　(38)　PERDEW J, BURKE K, E. M. Generalized Gradient Approximation Made Simple. *Phys. Rev.*

364　　　　*Lett.* **1996**, *77*, 3865–3868.

365　(39)　Parlinski, K.; Li, Z. Q.; Kawazoe, Y. First-Principles Determination of the Soft Mode in Cubic

366　　　　ZrO_2. *Phys. Rev. Lett.* **1997**, *78* (21), 4063–4066.

367　(40)　Togo, A.; Oba, F.; Tanaka, I. First-Principles Calculations of the Ferroelastic Transition

368　　　　between Rutile-Type and CaCl2-Type SiO_2 at High Pressures. *Phys. Rev. B* **2008**, *78* (13),

369　　　　134106.

370　(41)　Mao, H. K.; Xu, J.; Bell, P. M. Calibration of the Ruby Pressure Gauge to 800 Kbar under

371　　　　Quasi-Hydrostatic Conditions. *J. Geophys. Res.* **1986**, *91* (B5), 4673.

372　(42)　Prescher, C.; Prakapenka, V. B. DIOPTAS : A Program for Reduction of Two-Dimensional

373　　　　X-Ray Diffraction Data and Data Exploration. *High Press. Res.* **2015**, *35* (3), 223–230.

374　(43)　Toby, B. H. A Graphical User Interface for GSAS. *J. Appl. Crystallogr.* **2001**, *34*, 210–221.

375